Experimental Demonstration of Ultra-broadband Wireless Communications at True Terahertz Frequencies

Priyangshu Sen and **Josep M. Jornet**
Department of Electrical Engineering, University at Buffalo, The State University of New York
Buffalo, NY 14260, USA. E-mail: {priyangs, jmjornet}@buffalo.edu.

***Abstract*—In this paper, experimental results for wireless Terahertz (THz) communications at 1.02 THz, the first absorption-defined window above 1 THz, are presented. After briefly describing the hardware components of the experimental testbed, the details on the communication and signal processing algorithms, including synchronization, channel estimation and equalization, and modulation and demodulation, are described. The performance in terms of Bit Error Rate for single- and multi-carrier modulations able to support tens of Gigabits-per-second over sub-meter distances is presented and discussed, encouraging the exploration of communication systems at true THz frequencies.**

***Index Terms*—Terahertz communications; ultra-broadband networking; testbed and experimental research; beyond 5G**

I. Introduction

In the recent years, the way in which our society creates, shares and consumes information has lead to unprecedented growths in the number of wirelessly-connected mobile devices, the total amount of data that these devices generate and the speed at which they communicate [1]. In relation to the latter, following the current trend, Terabit-per-second (Tbps) links will become a reality within the next five years.

To enable Tbps links, different wireless technologies are being considered, ranging between massive MIMO communications at millimeter-wave (mm-wave) frequencies to optical wireless communications. In between the two ends of the electromagnetic (EM) spectrum, the Terahertz (THz) band (from 100 GHz to 10 THz) provides us with tens to hundreds of GHz of consecutive bandwidth and can potentially enable ultra-broadband wireless communication links [2].

Traditionally, the use of the THz band has been relegated to sensing and imaging applications due to the lack of both compact and efficient ways to generate, modulate and detect THz signals, as well as accurate models and understanding of the propagation of THz signals. However, major advancements from the device and communication perspectives are finally closing the THz gap. On the one hand, new electronic [3], photonic [4] and plasmonic devices [5] have demonstrated unprecedented performance in terms of operating frequency (meeting the 1 THz mark), power (up to tens and hundreds of mW) and modulation bandwidth (tens of GHz). On the other hand, accurate channel models based on radiative transfer theory have been developed for line-of-sight [6], and multi-path propagation [7].

In parallel to such developments, several experimental testbeds for THz communications have been developed. For example, experimental testbeds based on THz electronic devices have been demonstrated to support multi-Gigabit-per-second (Gbps) links over distances varying from less than a meter to hundreds of meters at 240 GHz [8] 300 GHz [9], 625 GHz [10] and 667 GHz [11], all still under 1 THz. Similarly, THz photonic devices have been utilized to create several platforms for ultra-broadband communications in the vicinity of 300 GHz [12], [13]. In all these platforms, the frequency is under 1 THz or in the sub-THz range. In order to study, understand and assess the feasibility of wireless communications at *true* THz frequencies, a platform able to support wireless links above 1 THz is needed.

In this paper, the TeraNova testbed, the world's first testbed at 1.02 THz is described and initial experimental results for wireless communications at true THz-band frequencies are provided. The paper is organized as follows. In Sec. II, we provide an overview of the hardware that integrates the THz testbed. In Sec. III, we describe the backbone of the platform, i.e., a software-defined physical layer in charge of synchronization, channel estimation and equalization, and modulation/demodulatiom. In Sec. IV, our experimental results in terms of link budget analysis, channel frequency characterization, noise power and phase characterization, and bit-error-rate (BER) for different modulation schemes, are provided and discussed. The paper is concluded in Sec. V.

II. TeraNova Hardware Overview

The TeraNova testbed and its corresponding block diagram are illustrated in Fig. 1. On the transmitter side, an analog signal generator (PSG, Keysight E8257D) with very low root mean square (RMS) jitter (21 fs) is utilized to synthesize the Local Oscillator (LO) at a frequency between 41.67 GHz and 43.75 GHz. A Schottky-diode-based chain of frequency multipliers, custom designed by Virginia Diode Inc. (VDI), is utilized to upconvert the LO to the target radio frequency (RF) between 1 THz and 1.05 THz. A mixer based on the same technology is utilized to mix an Intermediate Frequency (IF) signal generated by a state-of-the-art Arbitrary Waveform Generator (AWG, Keysight M8196A), with an analog bandwidth in excess of 32 GHz, a sampling frequency of up to 93.4 Giga-samples-per-second (GSas) and 8-bit resolution.

978-1-5386-6528-2/19/$31.00 ©2019 IEEE

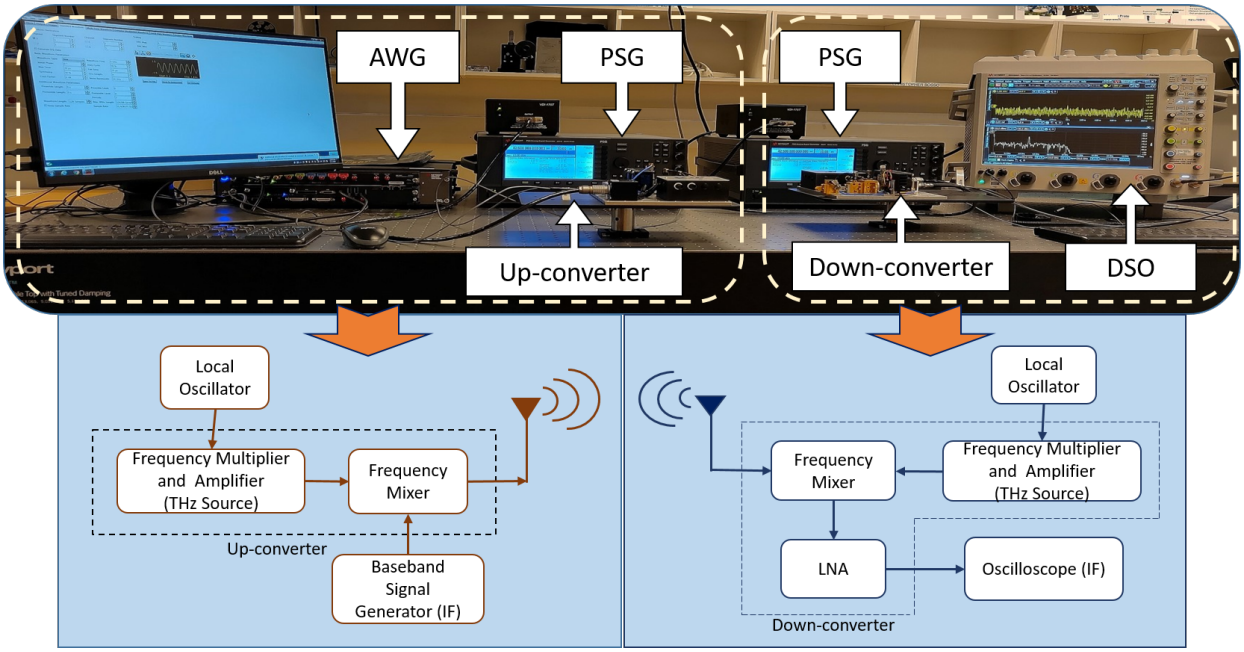

Fig. 1: The TeraNova testbed (top) and schematic diagram of the TeraNova transceiver hardware components (bottom).

The maximum input power at IF in the mixer is 0 dBm and the maximum output power is -15 dBm or 30 μW. On the receiver side, a second PSG and a frequency multiplier chain with mixer based on the same technology is utilized to generate the LO frequency and RF carrier, respectively, needed to down-convert the received RF frequency to IF band. A state-of-the-art Digital Storage Oscilloscope (DSO, Keysight DSOZ632A) with 63.2 GHz of bandwidth and 160 GSa of sampling frequency, is utilized to digitize, visualize and store the received signals for further processing. The software-defined physical layer (Sec. III) is utilized to Process the digitized signals. Furthermore, for transmitting and receiving the RF signal, two directional diagonal horn antennas (by VDI) are utilized. Both antennas exhibits 26 dBi gain and 10° angle half-power bandwidth at the 1 THz design frequency. Coaxial (2.4 mm male to male) and RoHS (restriction of hazardous substances) compliant cables are utilized to interconnect the different testbed elements.

III. TeraNova Software-Defined Physical Layer

In this section, we discuss the software-defined physical layer for the transceiver system, summarized in Fig. 2. At the transmitter, the data bits are organized in frames, modulated into symbols, and fed to the AWG. At the receiver, the digitized signals captured by the DSO are synchronized, equalized and demodulated to recover the data bits.

A. Frame Generation

The frame is composed of three parts: the header (a 20-bit-long predefined pseudo-random sequence), the training sequence (up to 200 bits) and the data sequence. The header is utilized to detect the beginning of a new frame and the training sequence is utilized for channel estimation and equalization purposes. The data sequence consists of 2184 user-defined bits.

B. Modulation

The generated frames are modulated according to single carrier and multi-carrier modulation schemes. In the case of single carrier modulation, M-ary Phase Shift Keying (M-PSK) is utilized, given by

$$I_m = \cos\left(\frac{(m-1)}{M}2\pi\right); Q_m = \sin\left(\frac{(m-1)}{M}2\pi\right), \quad (1)$$

where, (I_m) is in-phase and (Q_m) is quadrature components to generate the symbols.

Orthogonal frequency division multiplexing (OFDM) is utilized for multi-carrier modulation. The in-phase and quadrature components $(I_m + jQ_m)$ are modulated according to the data bits (for each carrier of OFDM) and passed through a serial to parallel conversion block, then fed to an IFFT block. Furthermore, the cyclic prefix is added to mitigate the effect of inter-symbol interference (ISI). To transmit the signal a parallel to serial conversion block is utilized. In the case of OFDM, frequency equalization is done by sending known $I_m + jQ_m$ values in regular carrier interval.

C. Pulse Shaping

A raised cosine pulse filter is utilized to modulate the symbol and restrict the generated signals' spectrum within the transmission bandwidth. The pulse-shaped signal is given by

$$x_m(t) = real[p(t)(I_m + jQ_m)]e^{(j2\pi f_{IF}t)}, \quad (2)$$

where t refers to time, p is the raised cosine pulse and f_{IF} refers to the intermediate frequency.

D. Pre-equalization

To compensate constant frequency selective response of the hardware components pre-equalization filter is implemented. In our case, this arises mainly from the frequency-dependent attenuation of the coaxial cables and connectors.

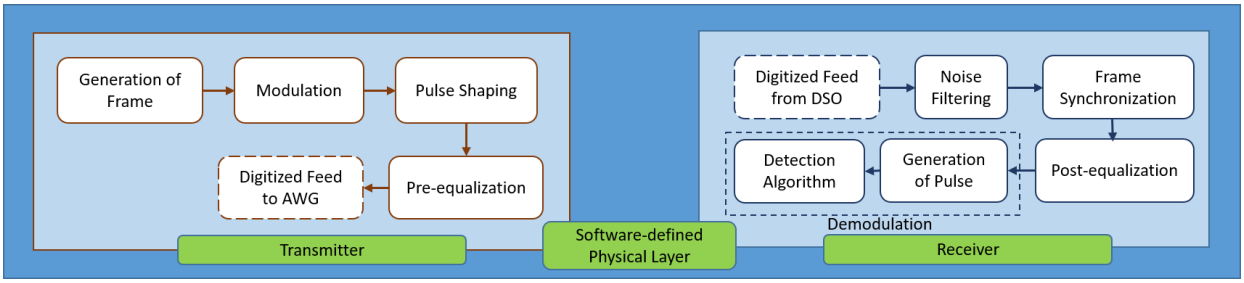

Fig. 2: Software-defined physical layer for The TeraNova platform

The frequency response $H(k)$ is calculated by comparing the transmitted and received single-tone IF signal within the system components bandwidth. The inverse of the frequency response is used as the frequency domain coefficient of the pre-equalization filter. The frequency response is given by

$$H(k) = \left(\frac{P_r(k) - P_n}{P_s(k)}\right)^{1/2}, \tag{3}$$

where $P_r(k)$ is the received signal power with noise at the k_{th} frequency, $P_s(k)$ is the transmitted signal power and P_n is the noise power for the whole observation bandwidth. Next, we describe the receiver implementation.

E. Noise Filtering

A Chebyshev bandpass filter based on Parks-McClellan-algorithm is utilized to remove the out of band noise to improve the performance.

F. Frame Synchronization

To synchronize with the starting point of the captured signal a correlator filter is utilized within the frame synchronization block. This block correlates the received signal with the same pseudo-random sequence utilized at the transmitter.

G. Post-equalization

To mitigate the effect of inter symbol interference (ISI), frequency selective nature of the channel and path loss a minimum mean square error (MMSE) based post-equalizer is utilized. In this case, end-to-end channel model is given by,

$$r(n) = h(n) * s(n) + v(n), \tag{4}$$

where $s(n)$ is the transmitted pilot signal to estimate the channel, $r(n)$ is the received signal, $v(n)$ are the noise samples and $h(n)$ are the channel coefficient. To design post-equalizing filter, we minimize the error between transmitted training signals and signals at output of the post-equalizer and given by,

$$\min||\hat{s} - R\hat{f}||^2 \; w.r.t \; \hat{f}, \tag{5}$$

Where $\hat{s}^T = [s(n+1)s(n+2)\ldots s(p)]$ is the transmitted pilot signal vector till the p_{th} instant; $\hat{f}^T = [f(0)f(1)\ldots f(n)]$ is the $n+1$ tap post-equalizer coefficient vector; and R $[(p-n)\times(n+1)]$ is Toeplitz matrix given by the following matrix,

$$\boldsymbol{R} = \begin{bmatrix} r(n+1) & r(n) & r(n-1) & \ldots & r(1) \\ r(n+2) & r(n+1) & r(n) & \ldots & r(2) \\ \vdots & \vdots & \vdots & \ddots & \vdots \\ r(p) & r(p-1) & r(p-2) & \ldots & r(p-n) \end{bmatrix}, \tag{6}$$

H. Demodulation

A correlator-type detector based on maximum likelihood (ML) criterion is utilized to recover the bits, as

$$\hat{m} = \underset{1\le m\le M}{\arg\max} \left(\int_0^T r(t)x_m(t)dt - \frac{1}{2}||x_m||^2 \right) \tag{7}$$

where $\hat{m}$ denotes the maximum match index and m=1,2,.... M (M is the modulation index). r represents the received symbol. x_m denotes all possible symbols generated (see Sec. III-C).

In the case of OFDM, the cyclic prefix is removed from the received symbol and passes through a serial to parallel conversion block to fed them an FFT block. At the output of the FFT block we get the corresponding complex baseband symbols in $I_m + jQ_m$ form and symbols are passed through detection algorithm for recovery of the bits.

IV. Experimental System Characterization and Tests Results

A. Link Budget Analysis

The received signal power P_{rx} in dB is given by

$$P_{rx} = P_{tx} + G_{tx} + G_{rx} + G_{LNA} - L_{spr} - L_{abs} - L_{mix} - L_{misc}, \tag{8}$$

where P_{tx} is the transmitted power, G_{tx} and G_{rx} are the transmit and receive antenna gains, respectively, G_{LNA} is the LNA gain at the receiver, L_{spr} refers the spreading loss, L_{abs} stands for the absorption loss, L_{mix} is the conversion loss at receiver and L_{misc} accounts for miscellaneous losses in cables and connectors. In Fig. 3, the estimated power and the actual received power for a 1.02 THz link are compared. The experimental results closely match with the theoretically computed values, which reinforce the system design.

B. Channel Frequency Characterization

The channel frequency is characterized by mixing a constant single tone IF of 1 GHz generated by the AWG and sweeping the LO frequency both at the transceiver in fixed steps of

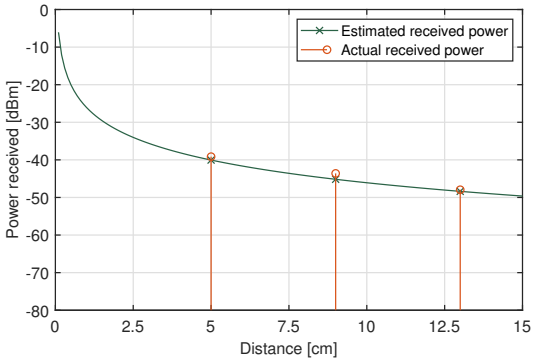

Fig. 3: Comparison of actual received power and estimated received power in different distance.

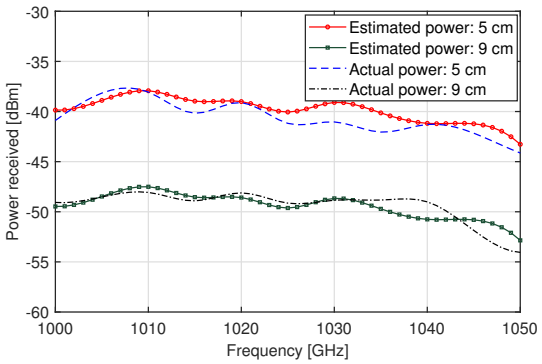

Fig. 4: Comparison of actual received power and estimated received power in different frequencies (1000 - 1050 GHz).

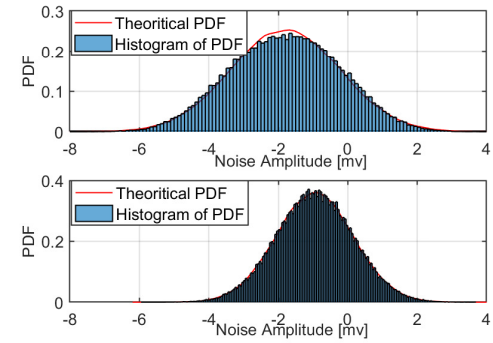

(a) Amplitude noise

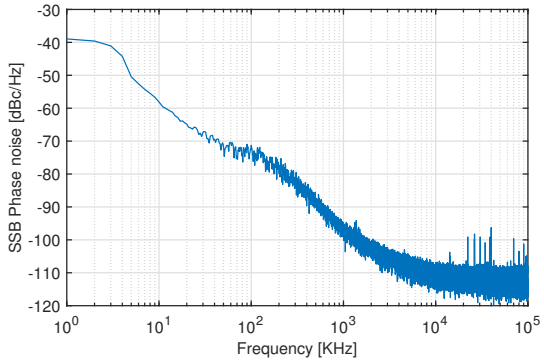

(b) Phase noise

Fig. 5: Comparison of PDFs of noise amplitude (top) and SSB phase noise for end to end transceiver system (bottom).

5 GHz, from 1 THz to 1.05 THz. In Fig. 4, we compare the measured channel frequency response with the analytical model, represented in [6]. The theoretically calculated and the experimentally measured values at 5 cm and 15 cm are close to each other.The results demonstrate the ultra-broadband response of the THz channel and devices, which opens the door to ultra-broadband communication systems at THz frequencies.

C. Noise Characterization

The main source of noise in our setup is the thermal noise at the receiver multiplier and mixer chain, in addition to the absorption noise introduced by water vapor molecules in the channel. Furthermore, low-frequency noise is introduced by the power supply and transmission chain.

The IF noise at the receiver for 62.3 GHz bandwidth is captured by the DSO (with and without the down-converter connected). In Fig. 5, It is observable by the graph, the histogram of the measured noise follows a Gaussian distribution, with approximated mean and variance given by -1.7 mv and 2.4 μw with the down-converter and -0.95 mv and 1.2 μw without the down-converter added, respectively.

Phase noise is rapid, short-term, random fluctuation in phase due to time domain instability, called jitter. The Single Side Band (SSB) Phase noise (comparing with the carrier power) of the end to end transceiver system is measured in terms of dBc/Hz. It reduced under -100 dBc/Hz after 1 MHz mark, which is illustrated in Fig. 5 and allow us to use different multicarrier modulation technique.

D. Data Communication

The performance of BPSK, QPSK, 8-PSK and OFDM at 1.02 THz, with modulation bandwidth of 10 GHz is experimentally tested. In the case of OFDM, 20 and 80 sub-carriers (SC) are utilized, modulated with BPSK symbols each having 500 MHz and 125 MHz bandwidth, respectively. In Table. I, we summarize our results in terms of BER by considering ten data frames (2,184-bit-long). It is observable that the BER increases for OFDM with the increase in the number of sub-carriers. Moreover, the performance of OFDM is unsatisfactory comaper to phase modulation. This is because of the peak-to-avg-power-ratio (PAPR) of OFDM is high and increases with the number of sub-carriers utilized, which reduce the detection capability of the low power component of the received signal. These results encourage the use of phase modulations for the current technology available.

In Fig. 6, the constellation diagram for BPSK, QPSK and 8-PSK modulation (13 cm distance) before and after equalization is plotted. Before equalization, the constellations are wide scattered than after equalization, which increases the BER. Moreover, equalization corrects the phase of the modulation.

In the Table II, BER with the decreasing number of pilot bits is illustrated for 8-PSK modulation (at 13 cm distance). The error rate increases as the number of pilot bits decreases.

Modulation	Distance (cm)	Bit rate(Gbps)	SNR(dB)	BER
BPSK	5	5	11.2	0
BPSK	9	5	8.1	0
BPSK	13	5	5.5	1.3×10^{-4}
QPSK	5	10	11.5	0
QPSK	9	10	8.2	4.5×10^{-5}
QPSK	13	10	5.7	5.5×10^{-4}
8-PSK	5	15	11	9.1×10^{-5}
8-PSK	9	15	7.8	4.6×10^{-3}
8-PSK	13	15	5.2	2.7×10^{-2}
OFDM	5	9.875 (80 SC)	17	9.1×10^{-4}
OFDM	9	9.875 (80 SC)	12.8	2.6×10^{-2}
OFDM	5	9.5 (20 SC)	16.8	8.2×10^{-4}
OFDM	9	9.5 (20 SC)	13	1.8×10^{-2}

TABLE I: BER for different modulation schemes at 1.02 THz.

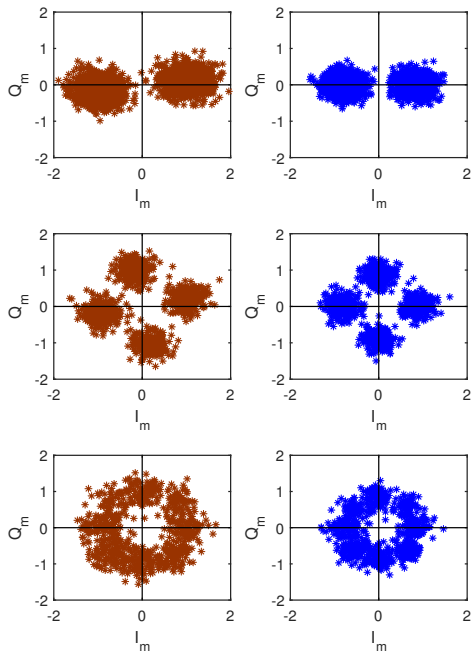

Fig. 6: Comparison of constellation diagram before and after equalization from left to right respectively, for BPSK (top), QPSK (middle) and 8-PSK (bottom) modulation.

No. of pilot bits	BER
201	2.7×10^{-2}
151	2.9×10^{-2}
101	3.0×10^{-2}
51	4.3×10^{-2}
15	0.1

TABLE II: BER with different number of pilot bits utilized for post-equalization, in case of 8-PSK received at 13 cm.

V. Conclusion

In this paper, we present the TeraNova testbed and software-defined backbone for ultra-broadband communication in frequency above 1 THz. This testbed will be the gateway to multi-Gbps as well as Tbps communication and long distance THz communication. The frequency characterization and noise statics of the channel have provided us with the in-site to use different modulation technique and power requirements for the successful communication. This setup opens up new avenues of research on ultra-high-speed data communication, signal processing and networking.

Acknowledgements

This work was supported by the U.S. National Science Foundation (NSF) under Grant No. CNS-1730148.

References

[1] Cisco, "Cisco visual networking index: Global mobile data traffic forecast update, 2017–2022," *White Paper*, Feb. 2019.

[2] I. F. Akyildiz, J. M. Jornet, and C. Han, "Terahertz band: Next frontier for wireless communications," *Physical Communication (Elsevier) Journal*, vol. 12, pp. 16–32, Sep. 2014.

[3] J. V. Siles, K. B. Cooper, C. Lee, R. H. Lin, G. Chattopadhyay, and I. Mehdi, "A new generation of room-temperature frequency-multiplied sources with up to 10× higher output power in the 160-ghz–1.6-thz range," *IEEE Transactions on Terahertz Science and Technology*, vol. 8, no. 6, pp. 596–604, 2018.

[4] T. Nagatsuma, G. Ducournau, and C. C. Renaud, "Advances in terahertz communications accelerated by photonics," *Nature Photonics*, vol. 10, no. 6, p. 371, 2016.

[5] A. C. Ferrari, F. Bonaccorso, V. Fal'Ko, K. S. Novoselov, S. Roche, P. Bøggild, S. Borini, F. H. Koppens, V. Palermo, N. Pugno *et al.*, "Science and technology roadmap for graphene, related two-dimensional crystals, and hybrid systems," *Nanoscale*, vol. 7, no. 11, pp. 4598–4810, 2015.

[6] J. M. Jornet and I. F. Akyildiz, "Channel modeling and capacity analysis for electromagnetic wireless nanonetworks in the terahertz band," *IEEE Transactions on Wireless Communications*, vol. 10, no. 10, pp. 3211–3221, 2011.

[7] C. Han, A. O. Bicen, and I. Akyildiz, "Multi-ray channel modeling and wideband characterization for wireless communications in the terahertz band," *IEEE Transactions on Wireless Communications*, vol. 14, no. 5, pp. 2402–2412, May 2015.

[8] I. Kallfass, F. Boes, T. Messinger, J. Antes, A. Inam, U. Lewark, A. Tessmann, and R. Henneberger, "64 gbit/s transmission over 850 m fixed wireless link at 240 ghz carrier frequency," *Journal of Infrared, Millimeter, and Terahertz Waves*, vol. 36, no. 2, pp. 221–233, 2015.

[9] C. Jastrow, S. Priebe, B. Spitschan, J. Hartmann, M. Jacob, T. Kürner, T. Schrader, and T. Kleine-Ostmann, "Wireless Digital Data Transmission at 300 GHz," *IET Electronics letters*, vol. 46, no. 9, pp. 661–663, 2010.

[10] L. Moeller, J. Federici, and K. Su, "2.5 Gbit/s duobinary signalling with narrow bandwidth 0.625 terahertz source," *Electronics letters*, vol. 47, no. 15, pp. 856–858, 2011.

[11] W. R. Deal, T. Foster, M. B. Wong, M. Dion, K. Leong, X. B. Mei, A. Zamora, G. Altvater, K. Kanemori, L. Christen *et al.*, "A 666 ghz demonstration crosslink with 9.5 gbps data rate," in *Microwave Symposium (IMS), 2017 IEEE MTT-S International*. IEEE, 2017, pp. 233–235.

[12] H.-J. Song, K. Ajito, Y. Muramoto, A. Wakatsuki, T. Nagatsuma, and N. Kukutsu, "24 Gbit/s data transmission in 300 GHz band for future terahertz communications," *IET Electronics letters*, vol. 48, no. 15, pp. 953–954, 2012.

[13] V. Chinni, P. Latzel, M. Zegaoui, C. Coinon, X. Wallart, E. Peytavit, J. Lampin, K. Engenhardt, P. Szriftgiser, M. Zaknoune *et al.*, "Single channel l00 gbit/s link in the 300 ghz band," in *2018 43rd International Conference on Infrared, Millimeter, and Terahertz Waves (IRMMW-THz)*. IEEE, 2018, pp. 1–2.